DCMIP2016, Part 1: Models and Equation Sets

Paul A. Ullrich[1], Christiane Jablonowski[2], James Kent[3], Peter H. Lauritzen[4], Ramachandran Nair[4], Kevin A. Reed[5], Colin M. Zarzycki[4], David A. Hall[6], Alex Reinecke[7], Kevin Viner[7], Don Dazlich[8], Ross Heikes[8], Celal Konor[8], David Randall[8], Xi Chen[9], Lucas Harris[9], Marco Giorgetta[10], Daniel Reinert[11], Christian Kuehnlein[12], Robert Walko[13], Vivian Lee[14], Abdessamad Qaddouri[14], Claude Girard[14], Hiroaki Miura[15], Tomoki Ohno[15], Ryuji Yoshida[16], Joseph Klemp[4], Sang-Hun Park[4], William Skamarock[4], Thomas Dubos[17], Yann Meurdesoif[17], Elijah Goodfriend[18], and Hans Johansen[18]

[1]University of California, Davis
[2]University of Michigan
[3]University of South Wales
[4]National Center for Atmospheric Research
[5]Stony Brook University
[6]University of Colorado, Boulder
[7]Naval Research Laboratory
[8]Colorado State University
[9]Geophysical Fluid Dynamics Laboratory
[10]Max Planck Institute for Meteorology
[11]Deutscher Wetterdienst (DWD)
[12]European Center for Medium-Range Weather Forecasting
[13]University of Miami
[14]Environment Canada
[15]University of Tokyo
[16]RIKEN
[17]Institut Pierre-Simon Laplace (IPSL)
[18]Lawrence Berkeley National Laboratory

Correspondence to: Paul A. Ullrich (paullrich@ucdavis.edu)

Abstract. This paper provides a comprehensive review of the design of modern non-hydrostatic atmospheric dynamical cores, including relevant equation sets, numerical stabilization techniques and idealized physics routines.

1 Introduction

INSTRUCTIONS FOR AUTHORS: Fill in text in section 3, 4, 5, 6, 7 and 8 below.

The Dynamical Core Model Intercomparison Project (DCMIP) is an ongoing effort targeting the intercomparison of a fundamental component of global atmospheric modeling systems: the dynamical core. Although this component's role is simply to solve the equations of fluid motion (the Naviér-Stokes equations) throughout the atmosphere, there are numerous confounding factors that arise as a consequence of compromises that are required to make simulation computationally feasible. These factors include the choice of model grid, vertical coordinates, representation of topography, numerical method, physics/dynamics coupler, and the manner in which artificial diffusion, filters and/or energy/mass fixers are applied.

To advance the intercomparison project and provide a unique educational opportunity for students, DCMIP has hosted a multidisciplinary two-week summer school and model intercomparison project, held at the National Center for Atmospheric Research (NCAR) in June 2016, that invited graduate students, postdocs, atmospheric modelers, expert lecturers and computer specialists to create a stimulating, unique and hands-on driven learning environment. It was built on previous intercomparison efforts by addressing key outstanding issues in global atmospheric models, incorporate international participation, and provide a unique training experience for the future generation of climate scientists. Special attention is paid to the role of simplified physical parameterizations, physics-dynamics coupling, non-hydrostatic atmospheric modeling and variable-resolution global modeling. The summer school and model intercomparison project promoted active learning, innovation, discovery, mentorship and the integration of science and education.

The summer school directly benefited its participants by providing a unique educational experience and an opportunity to interact with modeling teams from around the world. The workshop is expected to have further repercussions on the development of operational atmospheric modeling systems, by giving modeling groups an opportunity to assess and intercompare their models with other advanced modeling systems. Modeling groups have already begun to leverage this information to improve their own models, which will in turn positively impact the quality of weather and climate simulations going forward.

The proposed workshop has advanced our knowledge of (a) the relative behaviors exhibited by atmospheric dynamical cores, (b) differences that arise among mechanisms for coupling the physical parameterizations and dynamical core, and (c) the impacts of variable-resolution refinement regions and transition zones in global atmospheric simulations. Notably, the use of idealized test cases isolating specific phenomena gave us a unique opportunity to assess specific differences that arise due to the choice of dynamical core. A key outcome of the workshop was the development of a standard test case suite and benchmark set of simulations that can be used for assessment of any future dynamical core.

2 Notation

2.1 List of Symbols

Table 1 lists the symbols used in this paper.

2.2 List of Physical Constants

A list of physical constants which are used throughout this document is given in Table 2. Constants which are specific to each test case are similarly tabulated at the beginning of each section.

2.3 Great Circle Distance

The great circle distance is used throughout the document and is given by

$$R_c(\lambda_1, \varphi_1; \lambda_2, \varphi_2) = a \arccos\left(\sin\varphi_1 \sin\varphi_2 + \cos\varphi_1 \cos\varphi_2 \cos(\lambda_1 - \lambda_2)\right). \tag{1}$$

Table 1. List of symbols used in this manuscript

Symbol	Description
λ	Longitude (in radians)
φ	Latitude (in radians)
z	Height with respect to mean sea level (set to zero)
p_s	Surface pressure (p_s of moist air if $q > 0$)
Φ_s	Surface geopotential
z_s	Surface elevation with respect to mean sea level (set to zero)
u	Zonal wind
v	Meridional wind
w	Vertical velocity
ω	Vertical pressure velocity
δ	Divergence
ζ	Relative vorticity
p	Pressure (pressure of moist air if $q > 0$)
ρ	Total air density
ρ_d	Dry air density
T	Temperature
T_v	Virtual temperature
Θ	Potential temperature
Θ_v	Virtual potential temperature
q	Specific humidity
P_{ls}	Large-scale precipitation rate
q_c	Cloud water mixing ratio
q_r	Rain water mixing ratio

3 Model Grids

[ALL] Add a short description of your model grid here.

3.1 Latitude-longitude grid

3.2 Cubed-sphere grid

The equiangular cubed-sphere grid (Sadourny, 1972; Ronchi et al., 1996) consists of six Cartesian patches arranged along the faces of a cube which is then inflated onto a spherical shell. More information on this choice of grid can be found in Ullrich (2014). On the equiangular cubed-sphere grid, coordinates are given as (α, β, p), with central angles $\alpha, \beta \in [-\frac{\pi}{4}, \frac{\pi}{4}]$ and panel

Table 2. A list of physical constants used in this document.

Constant	Description	Value
a_{ref}	Radius of the Earth	6.37122×10^6 m
Ω_{ref}	Rotational speed of the Earth	7.292×10^{-5} s^{-1}
g_c	Gravitational acceleration	9.80616 m s^{-2}
p_0	Reference pressure	1000 hPa
c_p	Specific heat capacity of dry air at constant pressure	1004.5 J kg^{-1} K^{-1}
c_v	Specific heat capacity of dry air at constant volume	717.5 J kg^{-1} K^{-1}
R_d	Gas constant for dry air	287.0 J kg^{-1} K^{-1}
R_ν	Gas constant for water vapor	461.5 J kg^{-1} K^{-1}
κ	Ratio of R_d to c_p	$2/7$
ε	Ratio of R_d to R_ν	0.622
M_v	Constant for virtual temperature conversion	0.608
ρ_{water}	Reference density of water	1000 kg m^{-3}

index $i_p \in \{1,2,3,4,5,6\}$. By convention, we choose panels 1–4 to be along the equator and panels 5 and 6 to be centered on the northern and southern pole, respectively.

3.3 Icosahedral grid

3.4 Centroidal Voronoi tessellation grid

3.5 Octahedral reduced Gaussian grid

As with the classical reduced Gaussian grid of **?**, the octahedral reduced Gaussian grid (**??**) specifies the latitudes according to the roots of the Legendre polynomials. The two grids differ in the arrangement of the points along the latitudes, which follows a simple rule for the octahedral grid: starting with 20 points on the first latitude around the poles, four points are added with every latitude towards the equator, whereby the spacing between points along the latitudes is uniform and there are no points at the equator. The octahedral reduced Gaussian grid is suitable for transformations involving spherical harmonics, and has been introduced for global medium-range numerical weather prediction with the spectral dynamical core of the IFS at ECMWF in 2016. Figure 1 depicts the octahedral reduced Gaussian grid nodes together with the edges of the primary mesh as applied in the context of the finite-volume discretisation of FVM (Section 8.11).

4 Equation Sets

[ALL] Include the continuous equation set that you use for your model here.

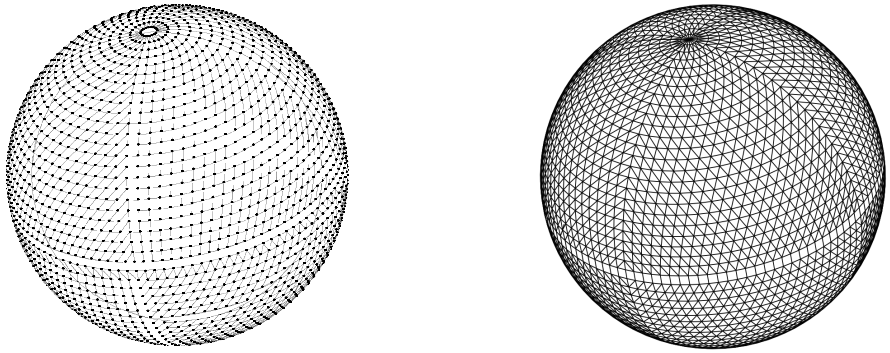

Figure 1. Locations of the octahedral reduced Gaussian grid nodes (left), and the edges of the primary mesh connecting the nodes as applied with the finite-volume discretisation in FVM (right). A coarse grid with only 24 latitudes between pole and equator is used for illustration. The dual mesh resolution of the octahedral reduced Gaussian grid is about a factor 2 finer at the poles than the equator; see **?**.

4.1 FVM

The fully compressible Euler equations solved in FVM are given as

$$\frac{\partial \mathcal{G}\rho_d}{\partial t} + \nabla \cdot (\mathbf{v}\mathcal{G}\rho_d) = 0 \,, \tag{2a}$$

$$\frac{\partial \mathcal{G}\rho_d \mathbf{u}}{\partial t} + \nabla \cdot (\mathbf{v}\mathcal{G}\rho_d \mathbf{u}) = \mathcal{G}\rho_d \left(-\Theta \widetilde{\mathbf{G}} \nabla \phi' - \frac{\mathbf{g}}{\theta_a} (\theta' + \theta_a(\epsilon q_v' - q_c - q_r)) - \mathbf{f} \times \left(\mathbf{u} - \frac{\theta}{\theta_a} \mathbf{u}_a \right) + \mathbf{M} \right) \,, \tag{2b}$$

$$\frac{\partial \mathcal{G}\rho_d \theta'}{\partial t} + \nabla \cdot (\mathbf{v}\mathcal{G}\rho_d \theta') = \mathcal{G}\rho_d \left(-\widetilde{\mathbf{G}}^T \mathbf{u} \cdot \nabla \theta_a - \frac{L}{c_p \pi} \left(\frac{\Delta q_{vs}}{\Delta t} + E_r \right) + \mathcal{H} \right) \,, \tag{2c}$$

$$\phi' = c_p \theta_0 \left[\left(\frac{R_d}{p_0} \rho_d \theta (1 + q_v/\varepsilon) \right)^{R_d/c_v} - \pi_a \right] \,, \tag{2d}$$

which describe the conservation laws of dry mass (2a), momentum (2b), and dry entropy (2c). Dependent variables in (2) are dry density ρ_d, three-dimensional physical velocity vector $\mathbf{u}$, potential temperature perturbation θ', and Exner pressure perturbation π', with the thermodynamic variables related by the gas law (2d) [1]. Mixing ratios of water vapor, cloud condensate, and rain are denoted as q_v, q_c, and q_r, respectively. All primed variables correspond to deviations from an ambient state (denoted by subscript "a") that satisfies a balanced subset of (2), thus $\psi' = \psi - \psi_a$, where $\psi = u, v, w, \theta, ..$; see **?** and **?**. The subscript "0" appearing with θ_0 refers to a constant reference value. Symbols appearing on the rhs of the momentum equation (2b) are the coefficient

$$\Theta := \frac{\theta\,(1 + q_v/\varepsilon)}{\theta_0\,(1 + q_t)} \tag{3}$$

in front of the pressure gradient term with Θ/θ_0 the density potential temperature, the gravity vector $\mathbf{g} \equiv (0, 0, -g)$ [2], the Coriolis parameter $\mathbf{f}$, and $\epsilon = 1/\varepsilon - 1$ with $\varepsilon = R_d/R_v$. The governing equations (2) are formulated with respect to a geospherical

[1] Note that ϕ' represents a normalised Exner pressure perturbation.

[2] In the shallow- versus deep-atmosphere form of the governing equations, gravity is constant $g \equiv g_c$ or varies with height as $g = g_c\,(a/r)^2$, respectively.

coordinate system and a generalised height-based terrain-following vertical coordinate [3]. Associated symbols are the Jacobian of the metric tensor $\mathcal{G}$, a matrix of metric coefficients $\widetilde{\mathbf{G}}$, its transpose $\widetilde{\mathbf{G}}^T$, and the transformation of the physical to the contravariant velocity $\mathbf{v} = \widetilde{\mathbf{G}}^T\mathbf{u}$; see **?** and **?** for discussion. The symbol $\mathbf{M}$ in (2b) subsumes metric forces due to the curvature of the sphere (**?**) and momentum dissipation, whereas $\mathcal{H}$ in (2c) represents the diffusion of heat.

4.2 Tempest

The continuity, momentum and thermodynamic equations can be written as:

$$\frac{\partial \rho}{\partial t} = -\nabla \cdot (\rho \mathbf{u}), \tag{4}$$

$$\frac{\partial \mathbf{u}}{\partial t} = -\nabla(K + \Phi) - \theta \nabla \Pi + \boldsymbol{\eta} \times \mathbf{u}, \tag{5}$$

$$\frac{\partial \theta_v}{\partial t} = -\mathbf{u} \cdot \nabla \theta_v, \tag{6}$$

in terms of Kinetic energy $K = \mathbf{u} \cdot \mathbf{u}$, geopotential $\Phi = g_c z$ and absolute vorticity $\boldsymbol{\eta} = \boldsymbol{\zeta} + \boldsymbol{\Omega}$, which consists of relative vorticity $\boldsymbol{\zeta} = \nabla \times \mathbf{u}$ and planetary vorticity $\boldsymbol{\Omega}$. The Exner pressure is related to the prognosed density and potential temperature via

$$\Pi = c_p \left(\frac{p_0}{p} \right)^{R_d/c_p} = c_p \left(\frac{R_d \rho \theta_v}{p_0} \right)^{R_d/c_v}. \tag{7}$$

4.3 Tracer transport

Lagrangian form:

$$\frac{dq}{dt} = 0. \tag{8}$$

Non-conservative Eulerian form:

$$\frac{\partial q}{\partial t} = -\mathbf{u} \cdot \nabla q. \tag{9}$$

Flux form:

$$\frac{\partial}{\partial t}(\rho q) = -\nabla \cdot (\rho q \mathbf{u}). \tag{10}$$

4.4 Height-based coordinates

Define Unstaggered, Lorenz and Charney-Phillips staggering here

4.5 Mass-based coordinates

5 Diffusion and Stabilization

[ALL] Include explicit diffusion and stabilization techniques that you have applied in the dynamical core here.

[3] For simplicity, the vertical coordinate is assumed to be time-independent in the current presentation.

5.1 Scalar viscosity

Scalar viscosity (direct):

$$\frac{ds}{dt} = \ldots + \nu \nabla \cdot \nabla s. \tag{11}$$

Scalar viscosity (conservative):

$$\frac{d}{dt}(\rho q) = \ldots + \nu \nabla \cdot (\rho \nabla q). \tag{12}$$

5.2 Smagorinsky eddy viscosity

5.3 Vector viscosity, divergence and vorticity damping

Vector viscosity:

$$\frac{d\mathbf{u}}{dt} = \ldots + \nu \nabla^2 \mathbf{u} \tag{13}$$

Divergence damping:

$$\frac{d\mathbf{u}}{dt} = \ldots + \nu_{div} \nabla (\nabla \cdot \mathbf{u}) \tag{14}$$

Vorticity damping:

$$\frac{d\mathbf{u}}{dt} = \ldots + \nu_{vort} \nabla \times (\nabla \times \mathbf{u}) \tag{15}$$

5.4 Hyperviscosity

Repeated application of the scalar and vector viscosity operators

6 Filters and Fixers

[ALL] Include explicit filters and fixers that you have utilized in the dynamical core here.

6.1 Mass borrowing (positive definite preservation)

6.2 Mass fixers

6.3 Energy fixers

7 Temporal Discretizations

[ALL] Describe the time-stepping scheme / temporal discretization employed by your dynamical core here.

7.1 Runge-Kutta

7.1.1 Ullrich-Kinnmark-Gray 5 step 3rd order scheme

Explicit terms are evolved using a Runge-Kutta method which supports a large stability bound for spatial discretizations with purely imaginary eigenvalues. This particular scheme is based on Kinnmark and Gray (1984a, b) and takes the form

$$\begin{aligned}
\psi^{(1)} &= \psi^{(0)} + \tfrac{\Delta t}{5} f(\psi^{(0)}), \\
\psi^{(2)} &= \psi^{(0)} + \tfrac{\Delta t}{5} f(\psi^{(1)}), \\
\psi^{(3)} &= \psi^{(0)} + \tfrac{\Delta t}{3} f(\psi^{(2)}), \\
\psi^{(4)} &= \psi^{(0)} + \tfrac{2\Delta t}{3} f(\psi^{(3)}), \\
\psi^{(5)} &= -\tfrac{1}{4}\psi^{(0)} + \tfrac{5}{4}\psi^{(1)} + \tfrac{3\Delta t}{4} f(\psi^{(4)}).
\end{aligned} \tag{16}$$

7.2 Semi-implicit time integration of the fully compressible Euler equations in FVM

In the following we provide an outline of the semi-implicit time stepping scheme for the fully compressible Euler equations in FVM (Section 8.11). A comprehensive discussion of the integration scheme can be found in **??** for dry dynamics; and in **?** and **?** for extensions to moist dynamics. The generic two-time-level second-order template algorithm employed in the integration is given as

$$\psi_{\mathbf{i}}^{n+1} = \mathcal{A}_{\mathbf{i}}(\widetilde{\psi}^n, \mathbf{V}^{n+1/2}, (\mathcal{G}\rho_d)^n, (\mathcal{G}\rho_d)^{n+1}) + 0.5\,\Delta t\, R^{\psi}|_{\mathbf{i}}^{n+1} \;, \quad \widetilde{\psi}^n \equiv \psi^n + 0.5\,\Delta t\, R^{\psi}|^n \;. \tag{17}$$

In (17), ψ represents the solution variable, R^{ψ} is the respective rhs, and $\mathcal{A}$ symbolises an advective transport operator assumed here to be the non-oscillatory finite-volume MPDATA (Multidimensional Positive Definite Advection Transport Algorithm) scheme (**??**) [4].

The integration of the system (2) can basically be divided into three steps. First, the homogenous mass continuity equation is integrated with $\psi \equiv \rho_d$, $\mathbf{V} \equiv \mathbf{v}\mathcal{G}$, and $R^{\rho_d} \equiv 0$ in (17). Second, the thermodynamic (2c), momentum (2b), and moisture equations enter (17) with $\psi = u, v, w, \theta', ...$, $\mathbf{V} \equiv \mathbf{v}\mathcal{G}\rho_d$, and the rhs R^{ψ} which is generally depending on all prognostic variables. A high degree of implicitness in the representation of the rhs forcings is achieved by inverting the overall discrete system (17) to obtain closed-form expressions for the velocity updates – the procedure is facilitated by the co-located arrangement of variables on the computational mesh. Retained on the rhs of the derived closed-form velocity expressions is the pressure gradient term. The third step in the solution procedure is to formulate an implicit boundary value problem for the pressure variable ϕ' using an evolutionary form of the equation of state (2d). An $\mathcal{O}(\Delta t^2)$ integration of this equation with a Euler backward template algorithm in the spirit of (17) leads a Helmholtz equation. The associated 3D elliptic boundary value problem is solved iteratively using a bespoke preconditioned Generalised Conjugate Residual approach (**??**). Nonlinearities in R^{ψ} and the solution-dependent coefficients of the Helmholtz problem are lagged behind and executed in an outer iteration.

[4] Furthermore, in (17) the vector index $\mathbf{i}$ denotes the spatial position on the computational grid, Δt is the time step size between levels n and $n+1$.

7.3 Semi-Implicit time integration

8 Dynamical Cores

In this section provide a short description (approximately 0.5 pages) of the dynamical core, focusing on unique features or design specifications. Do not include information on the physical parameterizations used by the modeling system. Make reference to the model grid employed from section 3, the specific equation set being discretized by the model in section 4, explicit numerical techniques for diffusion and stabilization in section 5, filters and fixers in section 6 and the temporal discretization in section 7.

8.1 Tempest

[ULLRICH]

The Tempest model (Ullrich, 2014; Guerra and Ullrich, 2016) uses a horizontal spectral element discretization and vertical staggered nodal finite element method based on the cubed-sphere grid with terrain-following height-based coordinate. The standard Eulerian equations are employed with moist density ρ, thermodynamic closure θ_v and tracer density ρq. These continuous equations are given in section 4.2. The implementation includes both fully explicit time integration, using the UKG53 scheme described in section 7.1.1, and implicit-explicit options, where horizontal terms are explicitly discretized and vertical terms are treated implicitly. Scalar hyperviscosity is employed for ρ, θ and tracer variables via repeated application of (11). Vector hyperviscosity is also applied by decomposing the horizontal vector Laplacian into divergence damping (14) and vorticity damping (15) terms. Both viscosity operations are applied after the completion of all Runge-Kutta sub-cycles.

8.2 High-Order Method Modeling Environment (HOMME)

[HALL]

8.3 Model for Prediction Across Scales (MPAS)

[SKAMAROCK]

8.4 Colorado State University Model (CSU)

[RANDALL]

8.5 Geophysical Fluid Dynamics Laboratory FV Cubed (GFDL-FV3)

[HARRIS]

8.6 Chombo

[JOHANSEN]

8.7 Naval Research Laboratory NEPTUNE Model

[VINER, REINECKE]

8.8 Global Environmental Multiscale (GEM) Model

[LEE]

8.9 Ocean-Land-Atmosphere Model (OLAM)

[WALKO]

8.10 DYNAMICO

[DUBOS]

8.11 Finite-volume module of the Integrated Forecasting System

The finite-volume module (FVM) of the Integrated Forecasting System (IFS) is developed at ECMWF (**?**). FVM solves the fully compressible Euler equations in geospherical coordinates. Both deep-atmosphere and shallow-atmosphere equations are available by means of simple switches. The formulation incorporates a generalised, optionally time-dependent, terrain-following vertical coordinate based on height. A centred two-time-level semi-implicit integration scheme is employed with 3D implicit treatment of acoustic, buoyant, and rotational modes (**?**). The associated 3D Helmholtz problem is solved iteratively using a bespoke preconditioned Generalised Conjugate Residual approach. The integration procedure uses the multidimensional flux-form Eulerian non-oscillatory MPDATA advection scheme (**??**). The horizontal spatial discretisation is fully unstructured finite-volume using the median-dual approach. This is combined with a structured-grid finite-difference approach in the vertical direction; see **?** for an exposition. In both the horizontal and the vertical discretisation, all prognostic variables are co-located. The median-dual finite-volume mesh in the horizontal is developed about the points/nodes of the octahedral reduced Gaussian grid (Section 3.5). The octahedral reduced Gaussian grid is also employed in the spectral dynamical core of the current operational IFS at ECMWF, which facilitates interoperability of the two formulations. However, we note that FVM is not restricted to this grid and offers capabilities towards a broad classes of meshes including adaptivity.

No explicit diffusion is applied in FVM for DCMIP, apart from the momentum dissipation and scalar diffusion required for some of the test cases, which is the vertical dissipation/diffusion in the planetary boundary layer parametrisation and the constant-coefficient second-order dissipation/diffusion in the supercell test. An absorbing layer in the first latitude ring around the poles is optionally used in the form of a Rayleigh-type forcing to the prognostic variables. The dynamics time step is adapted at every time step according to a given maximum advective CFL number (typically somewhat smaller than 1). The physics time step is identical to the dynamics time step.

8.12 Icosahedral Non-hydrostatic (ICON) Model

[GIORGETTA]

8.13 Nonhydrostatic ICosahedral Atmospheric Model (NICAM) Model

[MIURA]

9 Idealized Physical Parameterizations

9.1 Kessler Physics

The cloud microphysics update according to the following equation set:

$$\frac{\Delta\theta}{\Delta t} = -\frac{L}{c_p\pi}\left(\frac{\Delta q_{vs}}{\Delta t} + E_r\right) \tag{18}$$

$$\frac{\Delta q_v}{\Delta t} = \frac{\Delta q_{vs}}{\Delta t} + E_r \tag{19}$$

$$\frac{\Delta q_c}{\Delta t} = -\frac{\Delta q_{vs}}{\Delta t} - A_r - C_r \tag{20}$$

$$\frac{\Delta q_r}{\Delta t} = -E_r + A_r + C_r - V_r\frac{\partial q_r}{\partial z}, \tag{21}$$

where L is the latent heat of condensation, A_r is the autoconversion rate of cloud water to rain water, C_r is the collection rate of rain water, E_r is the rain water evaporation rate, and V_r is the rain water terminal velocity.

The pressure follows from the equation of state

$$p = \rho R_d T(1 + 0.61 q_v) \tag{22}$$

with p the pressure, ρ the density of moist air, R_d the gas constant for dry air, T the temperature and q_v the mixing ratio of water vapor. The equation is rewritten as a nondimensional pressure Π equation.

$$\pi = \left(\frac{p}{p_0}\right)^{\frac{R_d T}{cp}} \tag{23}$$

To determine the saturation vapor mixing ratio the Teten's formula is used,

$$q_{vs}(p,T) = \left(\frac{380.0}{p}\right)\exp\left(17.27 \times \frac{T - 273.0}{T - 36.0}\right) \tag{24}$$

The autoconvection rate (A_r) and collection rate (C_r) follow Kessler parametrization and are defined by:

$$A_r = k_1(q_c - a) \tag{25}$$

$$C_r = k_2 q_c q_r^{0.875} \tag{26}$$

With $k_1 = 0.001\text{s}^{-1}$, $a = 0.001\text{g.g}^{-1}$ and $k_2 = 2.2\text{s}^{-1}$

Deriving from Klemp and Wilhelmson (1978) description of cloud water,rain water and water vapor mixing ratios. they are define as followed:

$$q_c^{n+1} = \max(q_c^r - \Delta q_r, 0) \tag{27}$$

$$q_r^{n+1} = \max(q_r^r - \Delta q_r + S, 0) \tag{28}$$

where S is the sedimentation term and Δq_r is defined as

$$\Delta q_r = q_c^n - \frac{q_c^n - \Delta \mathrm{t} \max(A_r, 0)}{1 + \Delta \mathrm{t} C_r} \tag{29}$$

The Rain evaporation equation is defined similarly to Ogura and Takahashi (1971) description:

$$E_r = \frac{1}{\rho} \frac{\left(1 - \frac{q_v}{q_{vs}}\right) C(\rho q_r)^{0.525}}{5.4 \times 10^5 + \frac{2.55 \times 10^6}{p q_{vs}}} \tag{30}$$

With ventilation factor C define as

$$C_r = 1.6 + 124.9(\rho q_r)^{0.2046} \tag{31}$$

The liquid water terminal velocity is similar to Soong and Ogura (1973) description with a mean density adjustment as suggested by Kessler (1969):

$$V_r = 36349(\rho q_r)^{0.1346} \left(\frac{\rho}{\rho_0}\right)^{-\frac{1}{2}} \tag{32}$$

10 Surface Fluxes on an Aqua-Planet with Prescribed Sea Surface Temperatures

The forcing by surface fluxes from an idealized ocean is described in Reed and Jablonowski (2012) and is partly reproduced here. We use a model configuration which corresponds to an aqua-planet setup with prescribed sea surface temperatures (SSTs). This forcing by the surface fluxes is applied to the state variables in the lowermost model level using a partially implicit formulation to avoid numerical instabilities. Throughout this section we use the subscript a to denote variables defined on the lowermost model level.

The surface fluxes depend on the *drag coefficient* C_d, defined as

$$\begin{aligned} C_d &= C_{d0} + C_{d1}|\boldsymbol{v}_a| \quad \text{for } |\boldsymbol{v}_a| < 20 \text{ m s}^{-1} \\ C_d &= 0.002 \qquad\qquad\quad \text{for } |\boldsymbol{v}_a| \geq 20 \text{ m s}^{-1}, \end{aligned} \tag{33}$$

where C_{d0} and C_{d1} are 7.0×10^{-4} (unitless) and 6.5×10^{-5} s m^{-1}, respectively, and $|\boldsymbol{v}_a|$ is the magnitude of the horizontal wind at the lowermost model level. In terms of the zonal wind u_a and meridional wind v_a, it is defined as

$$|\boldsymbol{v}_a| = \sqrt{u_a^2 + v_a^2}. \tag{34}$$

For both evaporation and sensible heat the bulk coefficient is set to

$$C_E = C_H = 0.0011. \tag{35}$$

The formulation of the surface fluxes makes use of the height of the lowermost full model level z_a (in m). For pressure-based models, z_a can be expressed with the help of the hydrostatic equation in terms of pressure

$$z_a = \frac{R_d T_{\nu,a}}{g} \frac{(\ln p_s - \ln p_-)}{2}, \tag{36}$$

where $T_{\nu,a} = T_a(1 + 0.608 q_a)$ is the virtual temperature at the lowermost full model level and p_- is the edge pressure at the model level interface between the lowest and second lowest full model levels. This notation and all following equations assume that the temperature, horizontal wind components and the specific humidity in the physical parameterization package are co-located in both the vertical and horizontal directions, as is the case for the Lorenz grid. The height of the lowest full model level should ideally lie between 60-70m above the ground to make the results comparable to those in the literature.

As described in Reed and Jablonowski (2012), the surface fluxes can be written as

$$\frac{\partial \boldsymbol{v}_a}{\partial t} = -\frac{C_d |\boldsymbol{v}_a| \boldsymbol{v}_a}{z_a} \tag{37}$$

$$\frac{\partial T_a}{\partial t} = \frac{C_H |\boldsymbol{v}_a| (T_s - T_a)}{z_a} \tag{38}$$

$$\frac{\partial q_a}{\partial t} = \frac{C_E |\boldsymbol{v}_a| (q_{sat,s} - q_a)}{z_a}. \tag{39}$$

We note that the wind at the surface is taken to be zero and therefore does not appear explicitly in (37). In these equations T_s denotes the prescribed sea surface temperature (SST) and $q_{sat,s}$ is the saturation specific humidity defined by the Clausius-Clapeyron equation

$$q_{sat}(p) \approx \varepsilon \frac{e_s(T_s)}{p} \approx \frac{\varepsilon}{p} e_0^* e^{-(L/R_\nu)[(1/T_s)-(1/T_0)]}, \tag{40}$$

where e_0^* ($= 610.78$ Pa) is the saturation vapor pressure at $T_0 = 273.16$ K.

The final form of the surface fluxes will vary for models with other choices of prognostic variables. For example, if potential temperature Θ_a is used (38) takes the form

$$\frac{\partial \Theta_a}{\partial t} = \frac{C_H |\boldsymbol{v}_a| (T_s - T_a)}{z_a} \left(\frac{p_0}{p_a} \right)^{R_d/c_p} \tag{41}$$

where $p_0 = 1000$ hPa is a reference pressure. This conversion uses the assumption that the pressure is time-invariant when individual physics parameterizations are applied. For other choices of prognostic variables like $(\rho u)_a$, $(\rho v)_a$, $(\rho \Theta)_a$ and $(\rho q)_a$ the right-hand-side of (37), (41) and (39) would need to be multiplied by the density of the air ρ.

In order to ensure numerical stability, each of the aforementioned surface fluxes are applied via a semi-implicit operator. We demonstrate this procedure on the temperature evolution equation (38). First, the time derivative is expanded using a backward Euler operator,

$$\frac{T_a^{n+1} - T_a^n}{\Delta t} = \frac{C_H |\boldsymbol{v}_a^n| (T_s - T_a^{n+1})}{z_a}. \tag{42}$$

The superscripts n and $n+1$ represent the current time step (after the update from the large-scale condensation scheme) and the future time step, respectively. Note, that on the right-hand-side of the equation the only variable taken implicitly is T_a. $|\boldsymbol{v}_a^n|$ is evaluated at the current time step and C_H is constant. The equation can now be solved for T_a^{n+1}

$$T_a^{n+1} = \frac{T_a^n + C_H|\boldsymbol{v}_a^n|T_s\frac{\Delta t}{z_a}}{1+C_H|\boldsymbol{v}_a^n|\frac{\Delta t}{z_a}}. \tag{43}$$

Similar equations for $\boldsymbol{v}_a$ and q_a can be calculated

$$\boldsymbol{v}_a^{n+1} = \frac{\boldsymbol{v}_a^n}{1+C_d^n|\boldsymbol{v}_a^n|\frac{\Delta t}{z_a}} \tag{44}$$

$$q_a^{n+1} = \frac{q_a^n + C_E|\boldsymbol{v}_a^n|q_{sat,s}^n\frac{\Delta t}{z_a}}{1+C_E|\boldsymbol{v}_a^n|\frac{\Delta t}{z_a}}, \tag{45}$$

with the time-level dependent coefficient C_d^n. Notice that the second term in the numerator of (44) is absent in the case of the zonal and merdional wind. This is because the wind is set to zero at the surface.

10.1 Simplified Mixing in the Planetary Boundary Layer

The forcing by the planetary boundary layer is described in Reed and Jablonowski (2012) and is partly reproduced here. To parameterize the surface fluxes that impact the zonal velocity u, the meridional velocity v and moisture q we start with the time rate of change equations

$$\frac{\partial u}{\partial t} = -\frac{1}{\rho}\frac{\partial \rho\,\overline{w'u'}}{\partial z} \tag{46}$$

$$\frac{\partial v}{\partial t} = -\frac{1}{\rho}\frac{\partial \rho\,\overline{w'v'}}{\partial z} \tag{47}$$

$$\frac{\partial q}{\partial t} = -\frac{1}{\rho}\frac{\partial \rho\,\overline{w'q'}}{\partial z}. \tag{48}$$

Potential temperature, as opposed to temperature, is used in the boundary layer parameterization because the vertical profile of the potential temperature is a suitable indicator of static stability. This adds the time rate of change equation

$$\frac{\partial \Theta}{\partial t} = -\frac{1}{\rho}\frac{\partial \rho\,\overline{w'\Theta'}}{\partial z}. \tag{49}$$

Here u', v', w', Θ' and q' symbolize the deviations of the zonal velocity, meridional velocity, vertical velocity, potential temperature and specific humidity from their averages, respectively. The average is indicated by an overbar. Note, assuming pressure is held constant (which is a common assumption in physical parameterizations), the potential temperature time tendency can be converted back to a temperature tendency of the following form

$$\frac{\partial T}{\partial t} = -\frac{1}{\rho}\left(\frac{p}{p_0}\right)^{\kappa}\frac{\partial \rho\,\overline{w'\Theta'}}{\partial z}. \tag{50}$$

with the reference pressure $p_0 = 1000$ hPa.

The turbulent mixing is characterized by a constant vertical eddy diffusivity to represent Ekman-like profiles of boundary layers

$$\overline{w'u'} = -K_m \frac{\partial u}{\partial z} \tag{51}$$

$$\overline{w'v'} = -K_m \frac{\partial v}{\partial z} \tag{52}$$

$$\overline{w'\Theta'} = -K_E \frac{\partial \Theta}{\partial z} \tag{53}$$

$$\overline{w'q'} = -K_E \frac{\partial q}{\partial z}. \tag{54}$$

Here, K_m is the eddy diffusivity coefficient for momentum and K_E is the eddy diffusivity coefficient for energy and set equal to that for water vapor. In order to calculate the eddy diffusivity coefficients, the eddy diffusivity is matched to that for the surface flux calculated in Appendix 10 at the lowermost model level. To allow for a smooth transition above the boundary layer ($p_{top} = 850$ hPa) the diffusivity coefficients for momentum taper to zero as

$$\begin{aligned} K_m &= C_d|\boldsymbol{v}_a|z_a && \text{for } p > p_{top} \\ K_m &= C_d|\boldsymbol{v}_a|z_a \exp\left(-\left[\tfrac{p_{top}-p}{p_{strato}}\right]^2\right) && \text{for } p \le p_{top}. \end{aligned} \tag{55}$$

Here the constant p_{strato} determines the rate of decrease and is set to 100 hPa. K_E is defined by

$$\begin{aligned} K_E &= C_E|\boldsymbol{v}_a|z_a && \text{for } p > p_{top} \\ K_E &= C_E|\boldsymbol{v}_a|z_a \exp\left(-\left[\tfrac{p_{top}-p}{p_{strato}}\right]^2\right) && \text{for } p \le p_{top}. \end{aligned} \tag{56}$$

We suggest implementing the boundary layer scheme with an implicit temporal discretization to avoid numerical instabilities. The details of this discretization are somewhat complicated, and so we refer to implementation details in Appendix D of Reed and Jablonowski (2012). In addition, we supply the DCMIP modeling groups with the complete "simple-physics" package as used in the model CAM which can serve as a template routine.

11 Conclusions

TEXT

Author contributions. TEXT

Acknowledgements. DCMIP2016 is sponsored by the National Center for Atmospheric Research Computational Information Systems Laboratory, the Department of Energy Office of Science (award no. DE-SC0016015), the National Science Foundation (award no. 1629819), the National Aeronautics and Space Administration (award no. ??), the National Oceanic and Atmospheric Administration (award no. ??), the Office of Naval Research and CU Boulder Research Computing. This work was made possible with support from our student and postdoctoral

participants: Sabina Abba Omar, Scott Bachman, Amanda Back, Tobias Bauer, Vinicius Capistrano, Spencer Clark, Ross Dixon, Christopher Eldred, Robert Fajber, Jared Ferguson, Emily Foshee, Ariane Frassoni, Alexander Goldstein, Jorge Guerra, Chasity Henson, Adam Herrington, Tsung-Lin Hsieh, Dave Lee, Theodore Letcher, Weiwei Li, Laura Mazzaro, Maximo Menchaca, Jonathan Meyer, Farshid Nazari, John O'Brien, Bjarke Tobias Olsen, Hossein Parishani, Charles Pelletier, Thomas Rackow, Kabir Rasouli, Cameron Rencurrel, Koichi Sakaguchi, Gökhan Sever, James Shaw, Konrad Simon, Abhishekh Srivastava, Nicholas Szapiro, Kazushi Takemura, Pushp Raj Tiwari, Chii-Yun Tsai, Richard Urata, Karin van der Wiel, Lei Wang, Eric Wolf, Zheng Wu, Haiyang Yu, Sungduk Yu and Jiawei Zhuang. We would also like to thank Rich Loft, Cecilia Banner, Kathryn Peczkowicz and Rory Kelly (NCAR), Carmen Ho, Perla Dinger, and Gina Skyberg (UC Davis) and Kristi Hansen (University of Michigan) for administrative support during the workshop and summer school.

References

Guerra, J. E. and Ullrich, P. A.: A High-order Staggered Finite-Element Vertical Discretization for Non-Hydrostatic Atmospheric Models, Geoscientfic Model Development, doi:10.5194/gmd-2015-275, (in press), 2016.

Kessler, E.: On the distribution and continuity of water substance in atmospheric circulation, 1969.

Kinnmark, I. P. and Gray, W. G.: One step integration methods with maximum stability regions, Math. Comput. Simulat., 26, 87–92, doi:10.1016/0378-4754(84)90039-9, 1984a.

Kinnmark, I. P. and Gray, W. G.: One step integration methods of third-fourth order accuracy with large hyperbolic stability limits, Math. Comput. Simulat., 26, 181–188, doi:10.1016/0378-4754(84)90056-9, 1984b.

Klemp, J. B. and Wilhelmson, R. B.: The simulation of three-dimensional convective storm dynamics, J. Atmos. Sci., 35, 1070–1096, 1978.

Ogura, Y. and Takahashi, T.: Numerical simulation of the life cycle of a thunderstorm cell, Mon. Weather Rev., 99, 895–911, 1971.

Reed, K. A. and Jablonowski, C.: Idealized tropical cyclone simulations of intermediate complexity: a test case for AGCMs, J. Adv. Model. Earth Syst., 4, M04 001, doi:10.1029/2011MS000099, 2012.

Ronchi, C., Ianoco, R., and Paolucci, P. S.: The 'Cubed Sphere': a new method for the solution of partial differential equations in spherical geometry, J. Comput. Phys., 124, 93–114, doi:10.1006/jcph.1996.0047, 1996.

Sadourny, R.: Conservative finite-difference approximations of the primitive equation on quasi-uniform spherical grids, Mon. Weather Rev., 100, 136–144, doi:10.1175/1520-0493(1972)100<0136:CFAOTP>2.3.CO;2, 1972.

Soong, S.-T. and Ogura, Y.: A comparison between axisymmetric and slab-symmetric cumulus cloud models, J. Atmos. Sci., 30, 879–893, 1973.

Ullrich, P.: A global finite-element shallow-water model supporting continuous and discontinuous elements, Geosci. Model Dev., 7, 3017–3035, 2014.